Journal of Engineering Management and Systems Engineering
https://www.acadlore.com/journals/JEMSE

Geometrical Precision and Surface Topography of mSLA-Produced Surgical Guides for the Knee Joint

Paweł Turek*, Jakub Jakubiec

Faculty of Mechanical Engineering and Aeronautics, Rzeszów University of Technology, 35-959 Rzeszów, Poland

* Correspondence: Paweł Turek (pturek@prz.edu.pl)

Received: 07-01-2023 **Revised:** 08-13-2023 **Accepted:** 08-21-2023

Citation: P. Turek and J. Jakubiec, "Geometrical precision and surface topography of mSLA-produced surgical guides for the knee joint ," *J. Eng. Manag. Syst. Eng.*, vol. 2, no. 3, pp. 150–157, 2023. https://doi.org/10.56578/jemse020302.

Abstract: In this study, the precision of anatomical models and surgical guides pertaining to the knee joint, fabricated using the mSLA technique, was critically examined. The ITK-SNAP program was employed for the segmentation and reconstruction of knee joint anatomical structures, while surgical guide modelling was executed using the Siemens NX program. Subsequent fabrication of the models was accomplished with the Anycubic Photon Mono 4K MSLA 3D printer. An MCA II articulated arm equipped with a laser head, in conjunction with a TalyScan 150 profilometer, was utilized to gauge both the geometrical fidelity and surface roughness of the resulting models. Results indicated that the geometrical precision of these models remained within a tolerance of +/-0.3 mm. With regard to surface roughness, the Sa parameter was observed to lie between 2 and 2.5 µm.

Keywords: Reverse engineering; Precision; CAD modelling; Surgical guide; Knee joint

1 Introduction

Reverse engineering (RE) encompasses a broad spectrum of methods employed to transmute real objects into a virtual realm [1–3]. Central to this discipline are tasks encompassing data acquisition, geometric reconstruction, and the transformation of this data into a format amenable to Computer-Aided Design (CAD) systems. Applications of RE span a multitude of sectors, with notable implementations seen in aviation [4], the automotive industry [5], and architecture [6]. A medical pivot is also observed, where RE aids in geometrically reconstructing anatomical structures [7–9], facilitating implant designs [10–12], formulating surgical guides [13, 14], and scaffold construction [15]. In the realm of model fabrication derived from RE, additive methods (AM) predominantly find usage. Here, a 3D - CAD model saved as an STL file format serves as the foundational element. Before an object's fruition, it undergoes layer segmentation. The fabrication process of the model, when employing additive techniques, is characterized by sequential material deposition, with each layer contributing to the intended shape [16]. This technology's burgeoning relevance in the medical sphere has catalyzed its rapid advancement and broadened application horizons [17–19].

A meticulous assessment of geometrical accuracy and surface topology becomes paramount when medical models are synthesized using additive methods. Geometrical accuracy verification traditionally hinges on both optical and tactile measurement techniques, utilizing tools such as callipers [20], coordinate measuring machines [21], measuring arms [22], and either structural or laser light systems [23]. Horizontal scanning, reliant on point acquisition arranged linearly, dominates the surface roughness appraisal through profile methods [24]. Such scans predominantly occur along the x-axis, succeeded by a stipulated sampling adjustment on the y-axis. Given the incessant advent of novel methods and materials in 3D printing, the continual revalidation of geometric accuracy and surface topology is deemed necessary. As of current understanding, an anatomical structure's geometric accuracy tolerance sits at +/- 0.25 mm, predominantly focused on the craniofacial region [25, 26]. Extensive explorations into other skeletal structures remain sparse. When delving into surface topology, complexities amplify. For biocompatible materials, surfaces exhibiting an arithmetical mean height (Sa) of approximately 4 µm find optimal cell tolerance. A majority of implants, however, present surfaces with Sa values between 1-2 µm [27]. The research encapsulated in this article aims to furnish a preliminary evaluation of the Anycubic Photon Mono 4K MSLA 3D printer, emphasizing its prowess in crafting models of anatomical structures and surgical guides specific to the knee joint.

2 Methodology

The primary objective of this study centered on the design of surgical guides targeting the knee joint region. Models were subsequently crafted employing the mSLA technique, with subsequent comparisons made on their geometrical accuracy and surface roughness. These delineated templates were designated for use in femoral and tibial head resections. During the segmentation and reconstruction process facilitated by the ITK-SNAP software, models of the femur and tibial bones were procured in subgraph (a) of Figure 1. The segmentation process, employing thresholding methods, was utilized on DICOM data pixels, effectively delineating the bone structures of the knee joint in subgraph (b) of Figure 1. Concurrently, the incorporation of built-in functions permitted the removal of undesired elements and artefacts. Ensuing this, voids representing non-bone tissue areas were filled, serving to streamline the model's geometry in subgraph (c) of Figure 1.

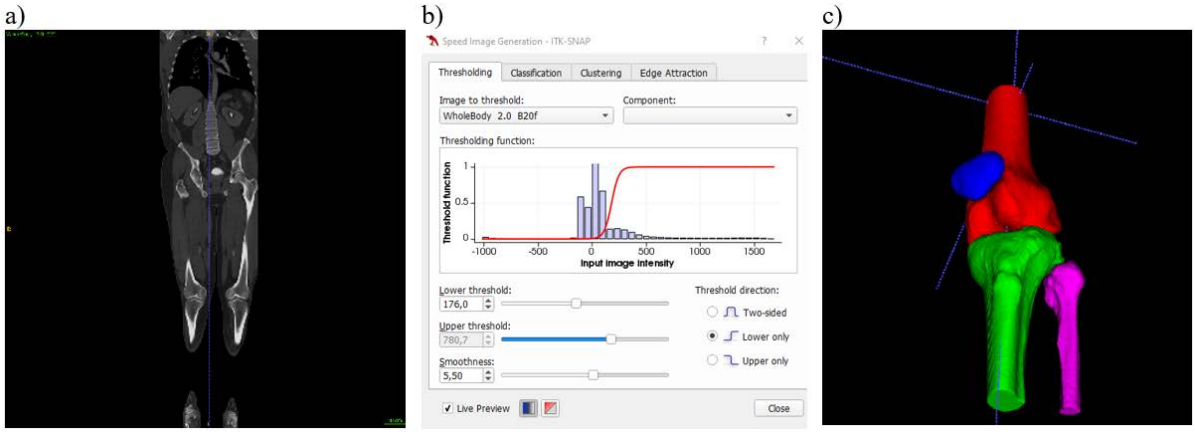

Figure 1. The 3D segmentation progression in ITK-SNAP: a) Assimilated image data; b) Determination of segmentation parameters; c) Resultant reconstructed models

The derived geometries of the femur and tibial bones were harnessed as foundational templates in the surgical guide design process. This comprehensive procedure leveraged hybrid modelling methodologies within the Siemens NX software. Drawing from the freeform surfaces of the bones and utilizing plane in subgraph (a) of Figure 2 and surface modelling tactics, the overarching form of the guides was synthesized in subgraph (b) of Figure 2. The design's fundamental tenet was predicated on forging contact points on bone shafts and the condyles situated atop the bone heads. This design stratagem was envisioned to guarantee apt guide positioning and to negate any potential dislodgment from the bones. Post the transformation of the surface model into a tangible solid entity via Boolean operations, the definitive model was formulated in subgraph (c) of Figure 2. During this modelling phase, emphasis was placed on ensuring a minimum of G1 continuity, aiming to render models with enhanced visual aesthetics. The apertures intended for guiding pins were affixed onto the bone's surface.

Following the design phase, CAD models of the surgical guides were exported to STL files, ensuring alignment with the specifications of the 3D printer. Parameters such as chordal tolerance were set at 0.005 mm, with an angular tolerance established at 5°. However, for the surgical guide model designed based on the tibial bone geometry, the chordal tolerance was adjusted to 0.0025 mm, the maximum value permitted by Siemens NX, to account for heightened precision requirements. STL files, which encapsulated the geometry of both the bones and surgical guides, were then fabricated using the Anycubic Photon Mono 4K MSLA 3D printer with Siraya Tech Fast resin as the chosen material. Notably, this resin lacks biocompatibility certification, yet possesses a heat deflection temperature of 65℃, making it suitable for low-temperature sterilisation (below 60℃), thus permitting its introduction into operating environments. The 3D printer in question employs an LCD screen to illuminate the resin, which is then separated from said screen via FEP foil. After curing each layer, the building platform transitions upwards. The exposure duration for each layer is contingent on the type of resin and its thickness. For this study, bone models and surgical guides were crafted with a layer thickness of 0.05 mm, and exposure times for individual layers were consistently maintained at 1.8 seconds. Support structures, automatically generated by the associated software, were deemed necessary for models created with this printer. Upon completion, the models were meticulously cleansed of resin remnants using 95% isopropyl alcohol, and support structures were delicately excised using a modelling scalpel. Subsequently, each model underwent final curing under natural UV light as shown in Figure 3.

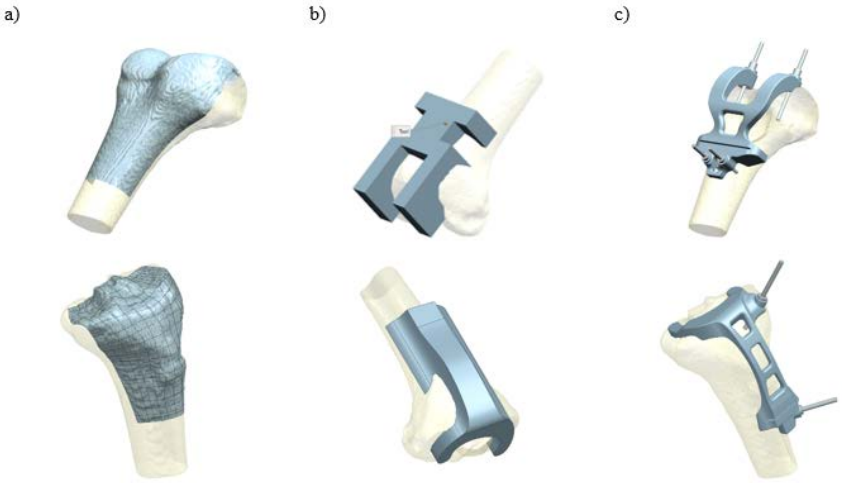

Figure 2. Surgical guide design progression: a) Bone surface replication; b) Genesis of form through surface modelling; c) Ultimate guide model rendition

Figure 3. Rendered models: a) Femur bone; b) Tibial bone; c) Surgical guide for femur bone; d) Surgical guide for tibial bone

The fidelity of the models' geometry was subsequently examined. The Metris Nikon MCA II measuring arm system, coupled with the MMD100 laser head, served as the primary apparatus for this endeavor in subgraph (a) of Figure 4. For comprehensive evaluation, scans of the models' geometry were bifurcated. Initially, the anterior section of the models was scrutinized in subgraph (b) of Figure 4, followed by the posterior segment. Throughout the assessment, a resolution of 0.01 mm was upheld. The intricate nature of each model necessitated multiple scans.

Surface texture was assessed employing the 3D profilometer, Talyscan 150 in subgraph (a) of Figure 5. A contact stylus was utilized to gauge the surface roughness parameters of the knee joint's anatomical models and the surgical templates in subgraph (b) of Figure 5. During this evaluation, a resolution of 5 µm was maintained, alongside the slowest feasible measurement velocity of 2,000 µm/s. Each assessed segment spanned an area of 4 mm×4 mm.

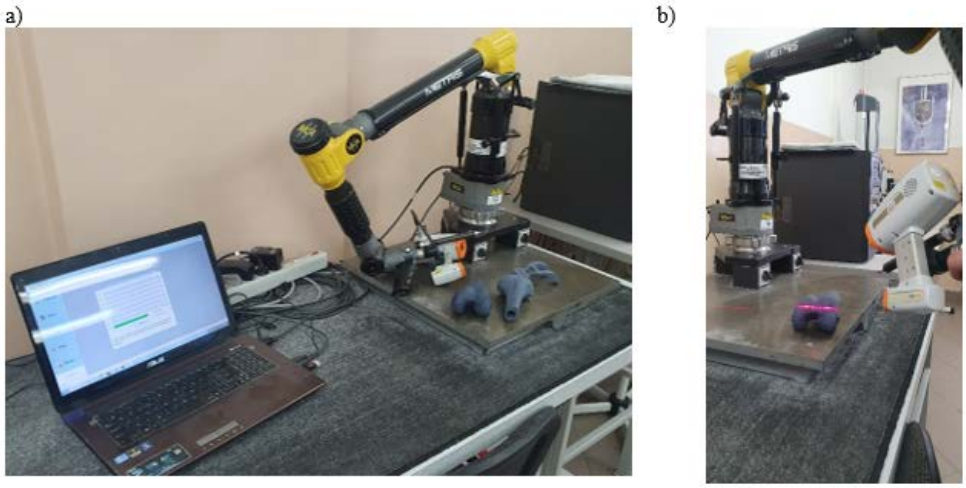

Figure 4. Geometry accuracy measurement: a) MCA-II measuring arm with the MMD×100 laser head; b) Assessment process

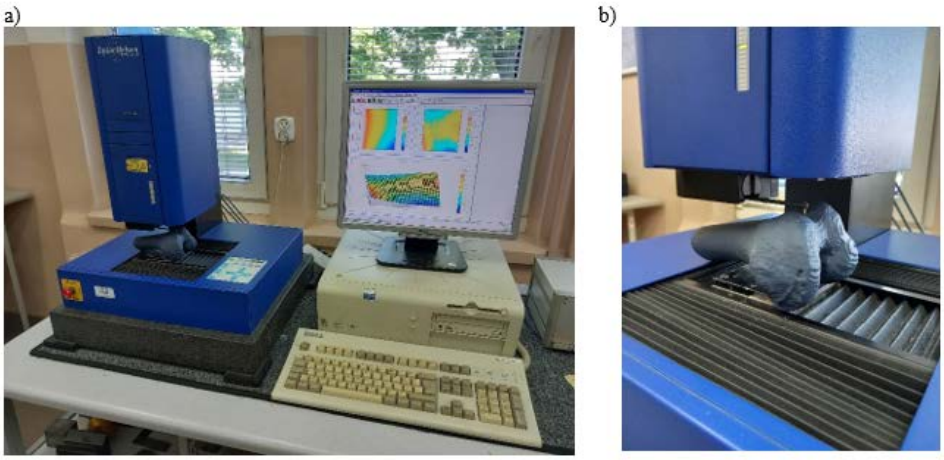

Figure 5. Surface texture assessment: a) Talyscan 150; b) Evaluation procedure

3 Results and Discussion

The accuracy of the models' geometry was verified utilizing the Focus Inspection software. In this validation, the best-fit method was employed, juxtaposing the nominal model—obtained during the design phase—to the reference model, derived from measurements executed with the MCA-II measuring arm and the MMD×100 laser head. Such alignments were achieved with an impressive precision of 0.001 mm. This process facilitated the creation of a three-dimensional deviation map, alongside fundamental statistical parameters to gauge geometry accuracy. Presented in Figure 6 reports that elucidate the geometry accuracy of the femur bone and the surgical guide, both of which were fabricated via mSLA technology.

A consistent pattern in deviation was discerned in particular regions of the examined geometries. Notably, an augmenting trend of negative deviations was identified, extending towards the periphery of the femur's anatomical model. The central region of the surface displayed deviations most congruent to the nominal value. A comparable pattern was noted for the surgical guide; however, a surge in positive deviations was detected along one edge of the model. For both models, negative deviations were predominant, with positive deviations exceeding 0.429 mm being localized. The most frequent deviation cluster ranged between -0.3 mm and -0.2 mm.

Surface roughness was appraised using the Mountains Map software. During the assessment, an initial filtration process was executed to eliminate form deviations. Subsequently, a profile filter $\lambda c = 0.8$ mm was utilized to segregate long-wave components, marking the boundary between roughness and waviness. Consequently, the resultant surface roughness was acquired. Based on the gathered data, the software further ascertained parameters such as Sa (arithmetical mean height), Sz (maximum height), Sp (maximum peak height), Sq (root mean square height), Sv

(maximum pit height), Ssk (skewness), and Sku (kurtosis), in alignment with the ISO 25178 – 2 standard [28]. Figure 7 showcases the surface roughness of the femur bone, created via mSLA technology. For subgraphs (a) and (c) of Figure 7, uniformity in structure was observed, as validated by the Sq, Ssk, and Sku parameters. The elevation in these parameter values for subgraph (b) of Figure 7 can be attributed to the removal of support material, manifesting as discernible surface damage. Despite this irregularity, the Sa parameter value remained in close proximity to the report in subgraph (c) of Figure 7. The surface parallel to the print layers yielded optimal results in the context of the evaluated attributes. Beyond its uniformity, this texture was characterized by the minimal Sa parameter value.

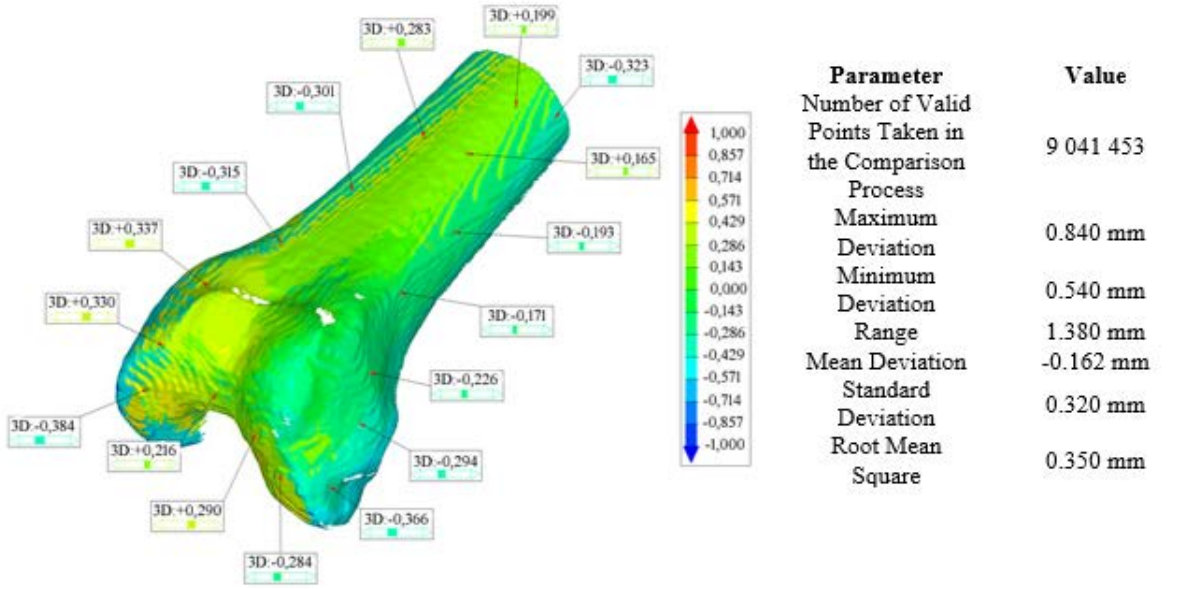

(a)

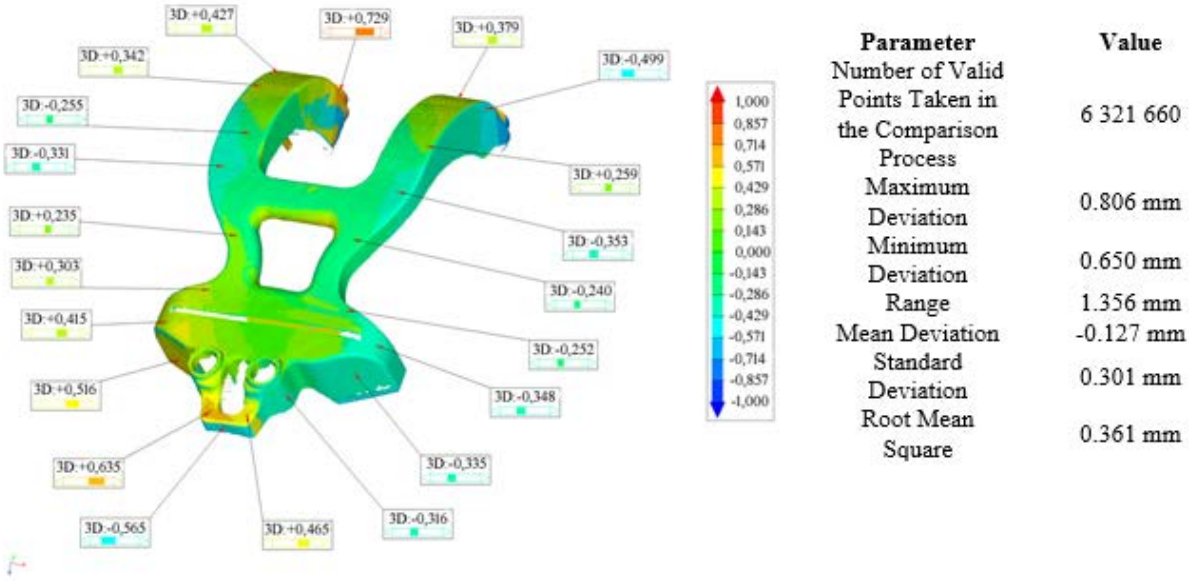

(b)

Figure 6. The reports on geometry accuracy: a) Femur bone; b) Surgical guide

A myriad of studies have been conducted to explore the correlation between manufacturing parameters and their subsequent effects on geometrical accuracy and surface roughness. Within the realm of mSLA methodologies, it has been identified that the photopolymerisation process [29], exposure strategies [30], and the projection system [31] play pivotal roles in determining the resultant surface quality. Surface roughness parameters, on the other hand, are predominantly influenced by factors such as the thickness of the print layer and the model's orientation within the 3D printer space [32]. It has also been observed that the chosen resin type exerts a significant impact on the final

outcomes. While the obtained results have been deemed satisfactory for surgical planning purposes, it is imperative to conduct further studies to elucidate the precise influence of selected 3D printing parameters on both geometrical accuracy and surface roughness.

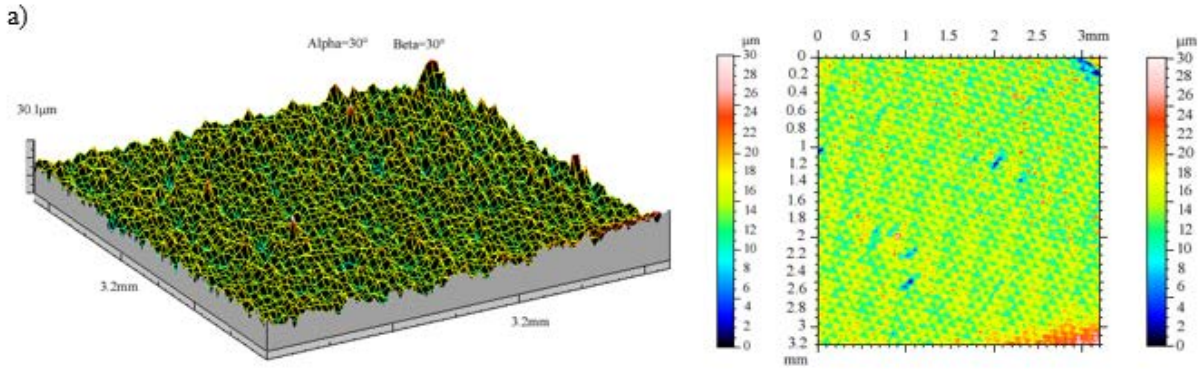

Parameter	Sa	Sz	Sp	Sv	Sq	Ssk	Sku
Value	2.07 µm	30.10 µm	15.30 µm	14.80 µm	2.69 µm	0.15	4.42

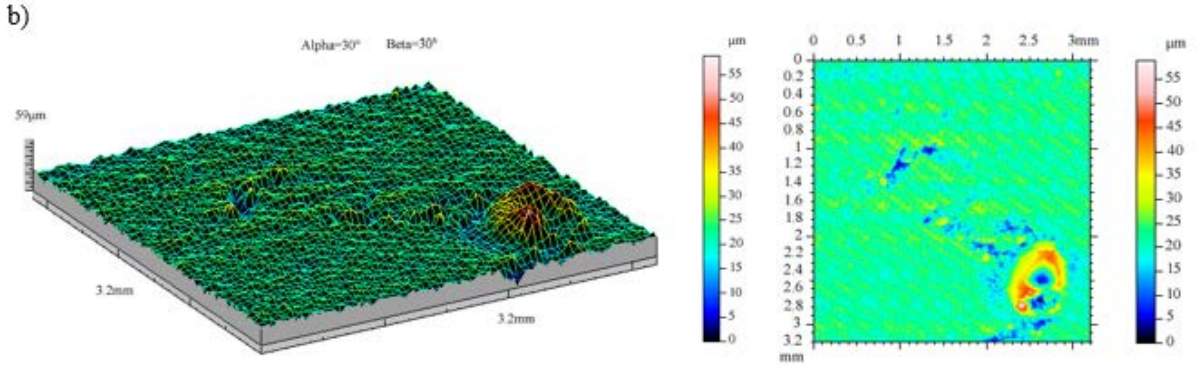

Parameter	Sa	Sz	Sp	Sv	Sq	Ssk	Sku
Value	2.55 µm	58.90 µm	36.80 µm	22.10 µm	3.88 µm	1.18	12.00

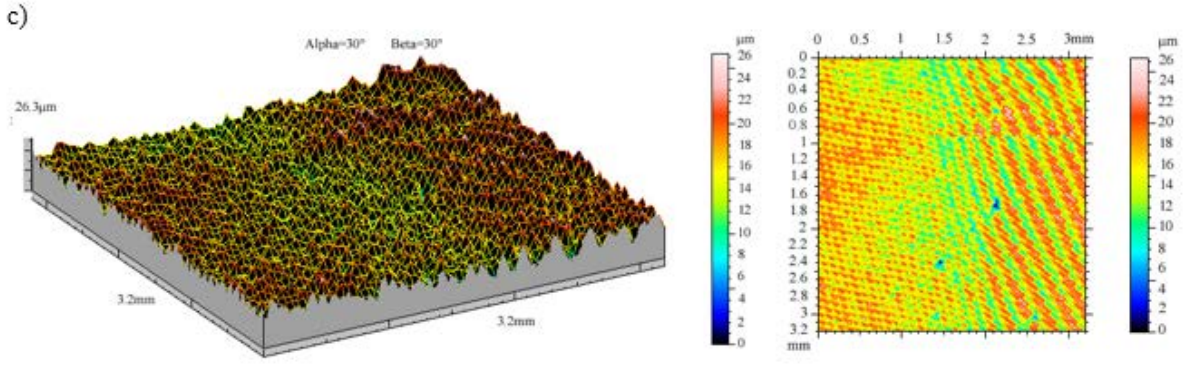

Parameter	Sa	Sz	Sp	Sv	Sq	Ssk	Sku
Value	2.59 µm	26.30 µm	10.50 µm	15.80 µm	3.19 µm	-0.11	2.69

Figure 7. a) Femur bone; b) and c) Variance due to support material removal

4 Conclusion

RE methodologies, in conjunction with additive techniques, have been effectively employed across diverse industrial sectors, notably in medicine. It is paramount that any resultant product adheres to specific criteria that

validate its proper implementation. In this context, assessments of geometrical accuracy and surface roughness are rendered indispensable. The parameters achieved in this study have been recognized as suitable for application in models utilized in surgical interventions, particularly within the knee joint region. The findings presented herein serve as a foundational basis for subsequent investigations, potentially delving into the domain of strength tests on the manufactured models.

Data Availability

The data used to support the findings of this study are available from the corresponding author upon request.

Conflicts of Interest

The authors declare that they have no conflicts of interest.

References

[1] A. Kumar, P. K. Jain, and P. M. Pathak, "Reverse engineering in product manufacturing: An overview," in *DAAAM International Scientific Book*, 2013, pp. 665–678. https://doi.org/10.2507/daaam.scibook.2013.39

[2] E. Bagci, "Reverse engineering applications for recovery of broken or worn parts and re-manufacturing: Three case studies," *Adv. Eng. Softw.*, vol. 40, no. 6, pp. 407–418, 2009. https://doi.org/10.1016/j.advengsoft.2008.07.003

[3] P. Turek and J. Jędras, "Precision analysis of chain wheel geometry reconstruction based on contact and optical measurement data," *J. Eng. Manage. Syst. Eng.*, vol. 2, no. 2, pp. 108–116, 2023. https://doi.org/10.56578/jemse020202

[4] I. G. E. Fedorova, T. S. Filimonova, E. V. E. Zhuravlev, and V. V. Vasiliev, "Estimation of the possibility of using reverse engineering in the aviation industry," *Comput. Nanotechnol.*, vol. 6, no. 3, pp. 68–73, 2019. https://doi.org/10.33693/2313-223x-2019-6-3-68-73

[5] M. Dúbravčík and Š. Kender, "Application of reverse engineering techniques in mechanics system services," *Procedia Eng.*, vol. 48, pp. 96–104, 2012. https://doi.org/10.1016/j.proeng.2012.09.491

[6] M. Acher, A. Cleve, P. Collet, P. Merle, L. Duchien, and P. Lahire, "Reverse engineering architectural feature models," in *Software Architecture: 5th European Conference, ECSA 2011, Essen, Germany*, pp. 220–235. https://doi.org/10.1007/978-3-642-23798-0_25

[7] P. Turek, "Evaluation of the auto surfacing methods to create a surface body of the mandible model," *Rep. Mech. Eng.*, vol. 3, no. 1, pp. 46–54, 2021. https://doi.org/10.31181/rme200103046p

[8] M. Stojkovic, M. Veselinovic, N. Vitkovic, D. Marinkovic, M. Trajanovic, S. Arsic, and M. Mitkovic, "Reverse modelling of human long bones using T-splines-case of tibia," *Tehnicki Vjesnik*, vol. 25, pp. 1753–1760, 2018. https://doi.org/10.17559/tv-20180129210021

[9] P. Turek, "Automating the process of designing and manufacturing polymeric models of anatomical structures of mandible with industry 4.0 convention," *Polimery*, vol. 64, no. 7-8, pp. 522–529, 2019. https://doi.org/10.14314/polimery.2019.7.9

[10] J. Milovanovic, N. Vitkovic, M. Stojkovic, and M. Mitkovic, "Designing of patient-specific implant by using subdivision surface shaped on parametrized cloud of points," *Tehnicki Vjesnik*, vol. 28, no. 3, pp. 801–809, 2021. https://doi.org/10.17559/tv-20200502215442

[11] N. Korunovic, D. Marinkovic, M. Trajanovic, M. Zehn, M. Mitkovic, and S. Affatato, "In silico optimization of femoral fixator position and configuration by parametric CAD model," *Materials*, vol. 12, no. 14, p. 2326, 2019. https://doi.org/10.3390/ma12142326

[12] M. Stojković, M. Trifunović, J. Milovanović, and S. Arsić, "User defined geometric feature for the creation of the femoral neck enveloping surface," *Facta Univ. Ser. Mech. Eng.*, vol. 20, no. 1, pp. 127–143, 2022. https://doi.org/10.22190/FUME200220034S

[13] L. Ciocca, S. Mazzoni, M. Fantini, F. Persiani, P. Baldissara, C. Marchetti, and R. Scotti, "A CAD/CAM-prototyped anatomical condylar prosthesis connected to a custom-made bone plate to support a fibula free flap," *Med. Biol. Eng. Comput.*, vol. 50, pp. 743–749, 2012. https://doi.org/10.1007/s11517-012-0898-4

[14] Y. F. Liu, L. W. Xu, H. Y. Zhu, and S. S. Y. Liu, "Technical procedures for template-guided surgery for mandibular reconstruction based on digital design and manufacturing," *Biomed. Eng. Online*, vol. 13, pp. 1–15, 2014. https://doi.org/10.1186/1475-925x-13-63

[15] J. Milovanović, M. Stojković, M. Trifunović, and N. Vitković, "Review of bone scaffold design concepts and design methods," *Facta Univ. Ser. Mech. Eng.*, vol. 21, no. 1, pp. 151–173, 2020. https://doi.org/10.22190/FUME200328038M

[16] I. Gibson, D. Rosen, and B. Stucker, *Additive Manufacturing Technologies*. Cham, Switzerland: Springer, 2021.

[17] M. Javaid and A. Haleem, "Additive manufacturing applications in medical cases: A literature based review," *Alex. J. Med.*, vol. 54, no. 4, pp. 411–422, 2018. https://doi.org/10.1016/j.ajme.2017.09.003

[18] P. Turek, K. Jońca, and M. Winiarska, "Evaluation of the accuracy of the resection template and restorations of the bone structures in the mandible area manufactured using the additive technique," *Rep. Mech. Eng.*, vol. 4, no. 1, pp. 39–46, 2023. https://doi.org/10.31181/rme040127022023t

[19] P. Turek and G. Budzik, "Development of a procedure for increasing the accuracy of the reconstruction and triangulation process of the cranial vault geometry for additive manufacturing," *Facta Univ. Ser. Mech. Eng.*, 2022.

[20] D. Ibrahim, T. L. Broilo, C. Heitz, M. G. de Oliveira, H. W. de Oliveira, S. M. W. Nobre, J. H. G. dos Santos Filho, and D. Nascimento Silva, "Dimensional error of selective laser sintering, three-dimensional printing and polyjet™ models in the reproduction of mandibular anatomy," *J. Cranio-Maxillofac. Surg.*, vol. 37, no. 3, pp. 167–173, 2009. https://doi.org/10.1016/j.jcms.2008.10.008

[21] M. Salmi, K.-S. Paloheimo, J. Tuomi, J. Wolff, and A. Mäkitie, "Accuracy of medical models made by additive manufacturing (rapid manufacturing)," *J. Cranio-Maxillofac. Surg.*, vol. 41, no. 7, pp. 603–609, 2013. https://doi.org/10.1016/j.jcms.2012.11.041

[22] P. Szymor, M. Kozakiewicz, and R. Olszewski, "Accuracy of open-source software segmentation and paper-based printed three-dimensional models," *J. Cranio-Maxillofac. Surg.*, vol. 44, no. 2, pp. 202–209, 2016. https://doi.org/10.1016/j.jcms.2015.11.002

[23] P. Turek and G. Budzik, "Estimating the accuracy of mandible anatomical models manufactured using material extrusion methods," *Polymers*, vol. 13, no. 14, p. 2271, 2021. https://doi.org/10.3390/polym13142271

[24] P. Turek, "Evaluation of surface roughness parameters of anatomical structures models of the mandible made with additive techniques from selected polymeric materials," *Polimery*, vol. 67, no. 4, pp. 162–167, 2022. https://doi.org/10.14314/polimery.2022.4.4

[25] A. Hazeveld, J. J. Huddleston Slater, and Y. Ren, "Accuracy and reproducibility of dental replica models reconstructed by different rapid prototyping techniques," *Am. J. Orthod. Dentofac. Orthop.*, vol. 145, no. 1, pp. 108–115, 2014. https://doi.org/10.1016/j.ajodo.2013.05.011

[26] K.-Y. Lee, J.-W. Cho, N.-Y. Chang, J.-M. Chae, K.-H. Kang, S.-C. Kim, and J.-H. Cho, "Accuracy of three-dimensional printing for manufacturing replica teeth," *Korean J. Orthod.*, vol. 45, no. 5, p. 217, 2015. https://doi.org/10.4041/kjod.2015.45.5.217

[27] R. Doornewaard, V. Christiaens, H. De Bruyn, M. Jacobsson, J. Cosyn, S. Vervaeke, and W. Jacquet, "Long-term effect of surface roughness and patients' factors on crestal bone loss at dental implants, a systematic review and meta-analysis," *Clin. Implant Dent. Relat. Res.*, vol. 19, no. 2, pp. 372–399, 2016. https://doi.org/10.1111/cid.12457

[28] *Geometrical Product Specifications (GPS). In Surface Texture: Areal—Part 2: Terms, Definitions and Surface Texture Parameters*, Std., 2012.

[29] R. Janusziewicz, J. R. Tumbleston, A. L. Quintanilla, S. J. Mecham, and J. M. DeSimone, "Layerless fabrication with continuous liquid interface production," *Proc. Natl. Acad. Sci.*, vol. 113, no. 42, pp. 11 703–11 708, 2016. https://doi.org/10.1073/pnas.1605271113

[30] J. V. Crivello and E. Reichmanis, "Photopolymer materials and processes for advanced technologies," *Chem. Mater.*, vol. 26, no. 1, pp. 533–548, 2013. https://doi.org/10.1021/cm402262g

[31] I. Kim, S. Kim, A. Andreu, J.-H. Kim, and Y.-J. Yoon, "Influence of dispersant concentration toward enhancing printing precision and surface quality of vat photopolymerization 3D printed ceramics," *Addit. Manuf.*, vol. 52, p. 102659, 2022. http://dx.doi.org/10.1016/j.addma.2022.102659

[32] A. Medellin, W. C. Du, G. X. Miao, J. Zou, Z. J. Pei, and C. Ma, "Vat photopolymerization 3D printing of nanocomposites: A literature review," *J. Micro Nano-Manuf.*, vol. 7, no. 3, 2019. http://dx.doi.org/10.1115/1.4044288